remote sensing

MDPI

Article

Flood Risk Assessment of Areas under Urbanization in Chongqing, China, by Integrating Multi-Models

Yuqing Li [1,2], Jiangbo Gao [1,2], Jie Yin [3,4], Lulu Liu [1,2], Chuanwei Zhang [1,2] and Shaohong Wu [1,2,*]

[1] Key Laboratory of Land Surface Pattern and Simulation, Institute of Geographic Sciences and Natural Resources Research, Chinese Academy of Sciences, Beijing 100101, China; liyuqing19@mails.ucas.ac.cn (Y.L.); gaojiangbo@igsnrr.ac.cn (J.G.); liull@igsnrr.ac.cn (L.L.); zhangcw.20b@igsnrr.ac.cn (C.Z.)
[2] University of Chinese Academy of Sciences, Beijing 100101, China
[3] Key Laboratory of Geographic Information Science, Ministry of Education, East China Normal University, Shanghai 200241, China; jyin@geo.ecnu.edu.cn
[4] School of Geographic Sciences, East China Normal University, Shanghai 200241, China
* Correspondence: wush@igsnrr.ac.cn

Abstract: In the context of urbanization, frequent flood event have become the most common natural disasters, posing a significant challenge to human society. Considering the effects of urbanization on flood risk is critical for flood risk reduction and reasonable land planning strategies at the city scale. This study proposes an integrated approach based on remote sensing data using CA, Markov, and simplified hydrodynamic (FloodMap) models to accurately and effectively assess flood risk under urbanization. Taking Chongqing City as a case study, this paper analyzes the temporal and spatial variations in land use/land cover (LULC) in 2010, 2015, and 2018 and predicts the LULC for 2030, based on historic trends. Flood risk is assessed by combining the hazard, exposure, and modified vulnerability. The results suggest that the area of built-up land will increase significantly from 19.56% in 2018 to 25.21% in 2030. From 2010 to 2030, the area of medium and high inundation depths will increase by 10 and 16 times, respectively. Flood damage varies remarkably according to the LULC and return period. The expected annual damage (EAD) has been estimated to increase from USD 68 million in 2010 to USD 200 million in 2030. Flood risk is proportional to population and is significantly inversely proportional to socioeconomic level. The approach used here can provide a comprehensive understanding of flood risk and is significant for land-use policymaking and the management of flood control facilities.

Keywords: LULC; flood risk; urbanization; socioeconomic; Chongqing; remote sensing data

Citation: Li, Y.; Gao, J.; Yin, J.; Liu, L.; Zhang, C.; Wu, S. Flood Risk Assessment of Areas under Urbanization in Chongqing, China, by Integrating Multi-Models. *Remote Sens.* **2024**, *16*, 219. https://doi.org/10.3390/rs16020219

Academic Editors: Prasad S. Thenkabail, Guangdong Li, Sanwei He and Zhiqi Yang

Received: 10 October 2023
Revised: 14 December 2023
Accepted: 30 December 2023
Published: 5 January 2024

1. Introduction

Floods are among the most common and destructive natural disasters worldwide IPCC [1,2]. The 2015 UNISDR report states that flood events constituted 47% of all weather-related disasters recorded between 1995 and 2015 [3]. These floods affected more than 2 billion people and contributed to economic losses of over USD 660 billion over the 2000–2012 period. China is one of the countries experiencing the most serious floods. Floods in China are characterized by high frequency, heavy losses, and long durations [4]. From 1950 to 2004, China experienced 125 significant floods, affecting 1.465 billion people and resulting in losses amounting to USD 11.675 billion [5]. Flooding costs account for 3.15% of China's annual gross national economic output [6]. Over the past few decades, the combined effects of climate change and urbanization have led to a rise in the occurrence of extreme rainfall, jeopardizing the lives and property of residents and causing increasing losses [7]. Thus, there is an urgent need to enhance flood risk assessment, enabling governments, emergency management agencies, and the public to prepare in advance and implement appropriate mitigation measures to reduce the threat of flood events to human life and property [8–10].

Generally, flood risk assessment considers hazards, exposure, and vulnerability [1,11,12]. Among these factors, exposure includes physical, environmental, and social assets; hazards refer to the probability and magnitude of flooding; and the potential adverse effects caused by exposure are expressed as vulnerability [13,14]. From 2000 to 2030, the amount of urban land located in high-frequency flood zones is estimated to increase by 30% globally [15]. Urbanization is usually accompanied by rapid land-use change, leading to changes in runoff, infiltration, groundwater recharge, and baseflow [16–18]. China has experience rapid global urbanization, with the rate increasing from 17.9% to 60.6% for the period of 1978–2019 [19]. Consequently, the increase in urban flooding has become a serious issue. To effectively and efficiently reduce flood losses and to develop and implement appropriate control strategies, an accurate flood risk assessment is necessary [20].

In recent years, flood risk assessments that include the dynamics of hazards, exposure, and vulnerability have received increasing attention [21–23]. In the analysis of future flood exposure and vulnerability, several studies utilize gridded economic/population data derived from Shared Socioeconomic Pathways (SSPs) [24–26]. However, the resolution of these data, often ranging from 1 km to 10 km, typically lacks the granularity required for detailed urban planning, particularly in rapidly urbanizing areas. This limitation can lead to an underestimation of future flood risks. To bridge this gap, higher-resolution and more explicit data are urgently needed to accurately capture the complexities of urbanization at the city scale. Remote sensing (RS) data can provide high-resolution images and spatially explicit data [27]. These data are available to the public in a cost-effective and efficient manner and are more suitable for land-use forecasting studies [28]. Land-use development models, such as cellular automata (CA) combined with artificial modeling, land-changed models based on GEOMOD, and agent-based models (ABMs), have been widely applied for future scenarios [29–31]. The CA-Markov model, in particular, is a robust method for dynamically modeling land use changes over space and time, efficiently integrating geographic information systems (GIS) and remote sensing data. This model is well-suited for simulating the spatial and temporal characteristics of complex systems at a fine spatial scale, which is crucial for mapping flood exposure and vulnerability [32–35]. Therefore, combining remote sensing data with sophisticated land-use models presents a vital solution for accurately assessing urban flood exposure and vulnerability.

The mapping of the flood hazard, a key component of risk assessments, mainly relies on various numerical models. Hydrodynamic models such as HEC-RAS and MIKE FLOOD, which are suited for simulating flow and water level in inland water bodies, demonstrate high simulation accuracy, but often at considerable computational costs [36]. On the other hand, hydrological models like HEC-HMS, designed for simulating precipitation runoff processes, are more cost-effective, but may lack the precision of hydrodynamic models [37]. This has led to the development and adoption of simplified models such as JFLOW, LISFLOOD-FP, and FloodMap [38–42]. These models reflect the dominant physics of flood processes and are input into the topography as a regular grid. Their performance has been shown to be similar to that of full 2D models in dealing with floods at a low computational cost. Particularly, the FloodMap model, improved by Yu and Coulthard [43], stands out for its enhanced capabilities. These developments allow for an efficient city-scale assessment of flood risk that integrates the future dynamics of hazard, exposure, and vulnerability.

This study develops an integrated approach combining the CA-Markov and FloodMap models to estimate the evolution of flood risk between 2010 and 2030 at a fine spatial scale, based on time series remote sensing data. Firstly, in order to model the future LULC under urbanization, we use CA-Markov models based on a high-precision LULC dataset, obtained from the Landsat satellite. Then, we simulate the inundation of floods under different LULC scenarios using Forest And Buildings removed Copernicus DEM (FABDEM) [44]. Combining CA-Markov with flood inundation models can provide higher accuracy and efficiency in urban flood risk assessment. This study implements this approach in Chongqing, China, which is experiencing rapid urbanization. This study also

examines the major factors impacting flood risk. The results, which identify and assess the risk of pluvial floods under urbanization scenarios, have practical applications for risk management and adaptation.

2. Study Area

Chongqing is a highly urbanized typical town located in southwestern China (28°10′–32°13′N and 105°11′–110°11′E), and its larger city region is selected as the study area. As shown in Figure 1, there are nine municipal districts in this study area: Yuzhong, Dadukou, Jiangbei, Shapingba, Jiulongpo, Nan'an, Beibei, Yubei, and Ba'nan. This area is the political, economic, and cultural center of Chongqing. According to statistical data for Chongqing, it covers about 5473 km^2 and has a population of 10.34 million people (https://data.cnki.net/yearbook (accessed on 22 May 2022)). It has grown rapidly in population and gross domestic product (GDP) since 1997 [45].

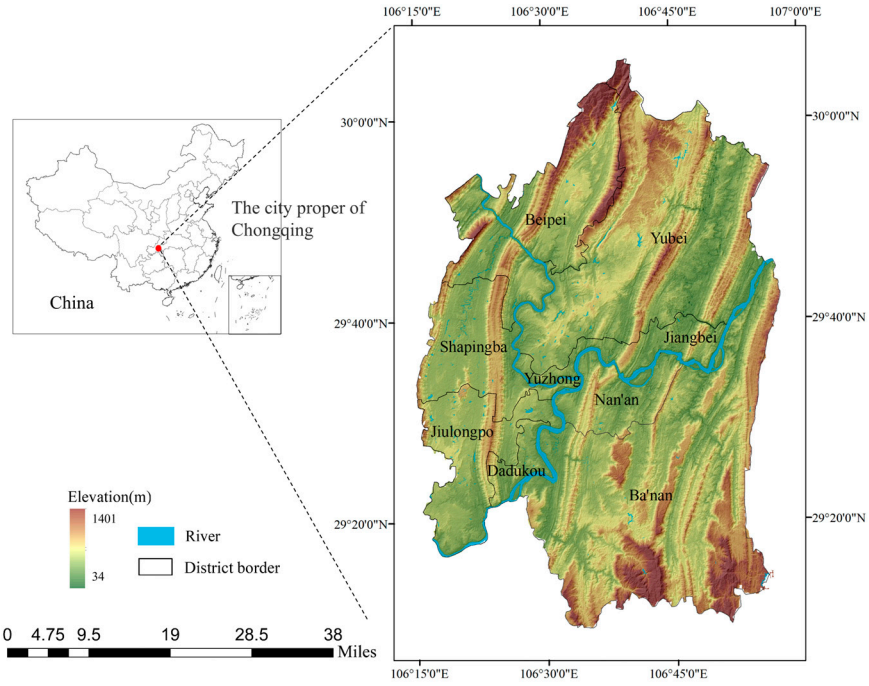

Figure 1. The study area of Chongqing City.

This study area has a typical subtropical monsoon climate characterized by four distinctive seasons, and the annual average rainfall is about 1148 mm. In the flood season from May to September, the precipitation accounts for 70% of the annual accumulation. Chongqing is a mountainous region in the middle and upper reaches of the Yangtze River, with typical complex topographic features [46]. From 2004 to 2019, this area experienced 364 heavy rain (a 24 h rainfall amount greater than 80 mm) and flood events, resulting in 763 deaths and disappearances. These disasters have caused a direct economic loss of USD 7.9 billion [47]. Recent years have seen an increase in rainstorms and an expansion of the scope of these disasters, leading to even higher economic losses. Based on the Yearbook of Meteorological Disasters from 2019 [48], the losses caused by pluvial floods accounted for more than 60% of the total meteorological disaster loss in 2018. Therefore, this study mainly focused on pluvial floods. This is an ideal case study for investigating and understanding the changes in flood risk influenced by rapid urbanization.

3. Data and Methods

3.1. Data Sources

For the purposes of this study, several remote sensing and survey datasets were chosen to model the changes in LULC and calculate the flood risk. The LULC dataset was acquired

from the Data Center for Resources and Environmental Science of the Chinese Academy of Sciences (http://www.resdc.cn/ (accessed on 22 May 2022)), obtained from Landsat satellite. This dataset is constructed through manual visual interpretation of cropland, woodland, grassland, water bodies, built-up land, and bare land, with a resolution of 30 m. The DEM was obtained from the work of Hawker et al. in 2022 [44]. FABDEM effectively mitigates the inherent biases arising from buildings and tree canopy height in conventional elevation data through remote sensing techniques and machine learning at a 30 m resolution. This dataset significantly improves terrain accuracy by reducing mean absolute error. The mean absolute vertical error of the dataset has been reduced to 1.12 m in urban areas and to 2.88 m in forests. This effectively enables the flooding model to explicitly capture and represent the shading effects of urban features. Population density data were collected from the Water Resources Planning Organization of China (https://www.worldpop.org (accessed on 2 May 2022)). The hydrometeorological data crucial for our study were sourced from the Chongqing Urban Rural Development Commission. This authoritative dataset provides comprehensive information on weather patterns, with a specific focus on rainfall statistics, in the Chongqing region [49].

The survey datasets were meticulously gathered to identify and analyze flood-prone points in Chongqing since 2018. We focused on several keywords regarding floodings to generate a set of media messages in the post-2018 context, which were then analyzed for various characteristics. The selected datasets underwent thorough identification, with emphasis on those providing detailed geographical coordinates and descriptions of the identified areas. To ensure the accuracy of our datasets, each location was verified by cross-referencing with multiple independent sources. This process yielded a refined collection of 29 distinct flood-prone locations, with each site's detailed information (Supplementary Materials—Table S1). These survey datasets are integral to our analysis, providing a reliable foundation for examining the flood susceptibility of these areas.

3.2. Methods

The overall framework of the future flood risk assessment is shown in Figure 2. First, this paper analyzed the temporal and spatial variations in LULC using remote sensing data with a single dynamic degree from 2010, 2015, and 2018, using GIS methods. The future LULC for 2030 was predicted using the CA-Markov model based on the historical trend. The flood risk, regarded as the potential for direct economic damage, was calculated as the combination of hazards, exposure, and vulnerability. We used the simplified hydrodynamic model (FloodMap) to simulate the flood inundation area and depth as flood hazards with return periods of 1 in 2, 10, 20, 50, and 100 years at different LULC periods. To increase the applicability of the exposure and vulnerability, depth–damage curves and land values were revised for Chongqing. All values in this paper are based on 2010 standards. Based on the damage model, we calculate flood losses for different return periods in 2010, 2015, 2018, and 2030. The expected annual damage (EAD) under different periods was also estimated to represent the flood risk under urbanization. Although flood risk estimates are associated with large uncertainties, our main interest was in identifying the changes at the urban microscale, which is more robust and exact than either global or regional scale estimates. The results are quantitative assessments of the economic losses in the flooded area, which were used to analyze any correlations with socioeconomic factors.

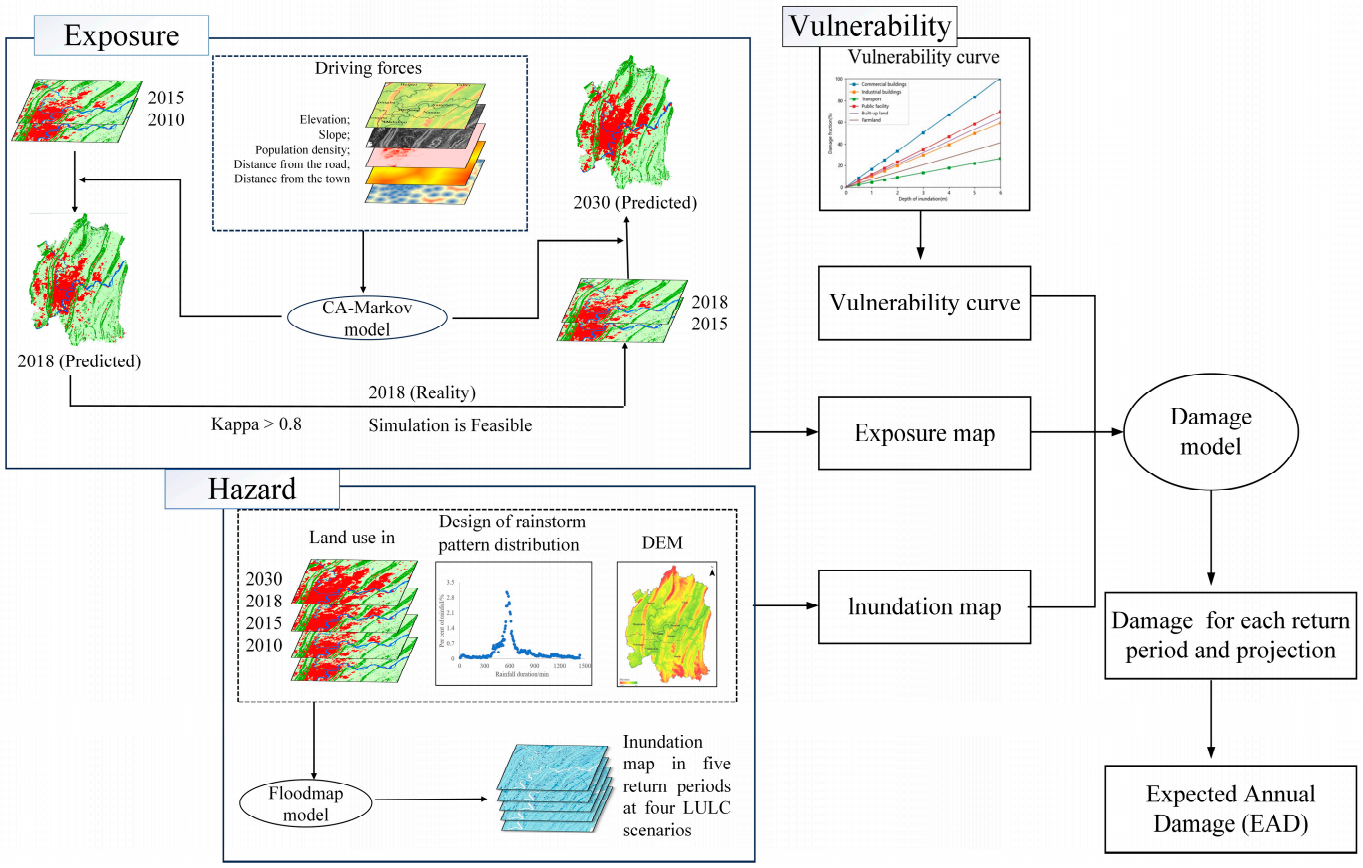

Figure 2. The overall framework of scenario-based future flood risk assessment.

3.2.1. Flood Exposure and Vulnerability Analysis

Flood Exposure

Flood exposure represents the degree to which a specific area or asset is at risk from flooding. In this study, we have chosen the value of land use as a key indicator for assessing flood exposure. Therefore, we employ the CA-Markov model for simulating the LULC in 2030. The CA-Markov model, which combines a Markov chain and cellular automata, is useful for simulating and predicting land-use changes [32,50]. This model can simulate changes over time and space, helping to determine the likelihood of transitions between different land use states [33]. The Markov transition process utilizes the following formula:

$$S_{t+1} = S_t \times P_{ij} \quad (1)$$

where S_t is the system status at time t; S_{t+1} is the system status at time $t+1$. P_{ij} is the transition probability matrix of a state, which is estimated as follows:

$$P_{ij} = \begin{pmatrix} P_{11} & \cdots & P_{1n} \\ \vdots & \ddots & \vdots \\ P_{n1} & \cdots & P_{nn} \end{pmatrix} \quad (2)$$

where P is the transition probability; P_{ij} stands for the probability of converting from the current state i to another state j in the next time point; and P_{nn} is the state probability of any time point.

Equation (3) shows the expression of the CA model.

$$S_{t+1} = f(S_t, N) \quad (3)$$

where S_t, S_{t+1} is the system status at time $(t, t+1)$; the function is the state probability of any time (N).

The obtained LULC is employed to simulate and predict future land changes using the CA–Markov model within IDRISI Selva 17.0 software. The specific process is as follows:

(1) Determining the transition rules

With Markov chain analysis, a matrix of transition probabilities observed between maps from 2010 and 2015 can be used to project future changes in regards to current patterns. Through spatial overlay analysis, the transition probability matrix and the transfer area of the matrix are achieved. The calculated transition probability matrix will serve as the transformation rules for putting CA–Markov model simulations into practice. Transition suitability maps were calculated using the multi-criteria evaluation (MCE) model, considering environmental and socioeconomic factors. The analytic hierarchy process (AHP) is the primary weighting method used for MCE. The weighted impacts of all selected factors for each cell were combined linearly in order to form a land suitability map. Based on the knowledge derived from the literature and from experts, factors including slope, elevation, distance from the road, distance from the town, and population density were considered to produce transition suitability maps [34,51].

(2) Determining CA filters and the number of iterations

CA filters can produce a clear sense of the space weighting factor, which can be changed according to the current adjacent cellular state. The standard 5×5 contiguity filter is used as the neighborhood definition in this study, and the simulation time step is 1 year. Six land-use types are considered in the model, and the size of the cell space in the CA model is set to 30 m $\times$ 30 m. The number of CA iterations is selected at 15 in order to simulate the landscape spatial pattern for the study area in 2030.

The model was validated for the year 2018. Therefore, considering the LULC maps for 2010 and 2015 as the initial and final state maps, the model predicted an LULC map for 2018. We compared the agreement between the observed and predicted geographic maps based on the Kappa statistic. In brief, Kappa is based on the percentage of agreement between two maps and corrects for the portion of this agreement that is due purely to chance. An accurate Kappa statistic is calculated using the following equation [52]:

$$\text{Kappa coefficient} = \frac{(T \times C) - G}{T^2 - G} \quad (4)$$

where T is the test pixels, C is the correctly classified pixel observations, and G is the sum of the multiplied total value. A value closer to 1 implies a more perfect agreement.

The degree of land-use dynamics can be used to quantify regional differences to describe the rate of land-use change [53]. The degree of a single land-use dynamic is calculated by the net value of the change in area of a single land-use type:

$$k = \frac{A_{t2} - A_{t1}}{A_{t1}} \times \frac{1}{t_2 - t_1} \times 100\% \quad (5)$$

where k is the dynamic degree of a single land-use type. The closer the value of k is to 1, the more marked the land-use change. A_{t2} represents the area of a certain type of land use at an earlier date, and A_{t1} represents the unchanged part. t_1 and t_2 represent the year before and after the change. We quantify and compare the dynamic changes in land use from 2010 to those predicted in 2030 to identify areas with rapid development.

Flood Vulnerability

Vulnerability is typically expressed as a depth–damage function. Yin (2011) [54] constructed curves for seven different land-use classes in Shanghai. To convert these (residential, transport, commercial, and public building curves) into a single curve for the built-up land-use category, we adopted the area-weighted average method, based on the

area of the different land-use categories (Figure 3) [55]. The depth–damage curve for cropland is consistent with that of Yin (2011) [54]. To increase the applicability of the land values for exposure, we calculated a correction factor based on the GDP and areas of Chongqing and Shanghai following the suggestion of Feng (2017) [56], which is 0.037. Based on the methods described above, we propose that the land-use distributions in Shanghai and Chongqing demonstrate a similar susceptibility to floods when the established exposure and vulnerability functions in Shanghai are adapted for use in Chongqing, after the application of their respective correction factor. In ArcGIS, the integration of land value data with inundation depth maps and vulnerability curves is achieved through spatial connections and merging tools, enabling the calculation of flood risk indices and the visualization of the results.

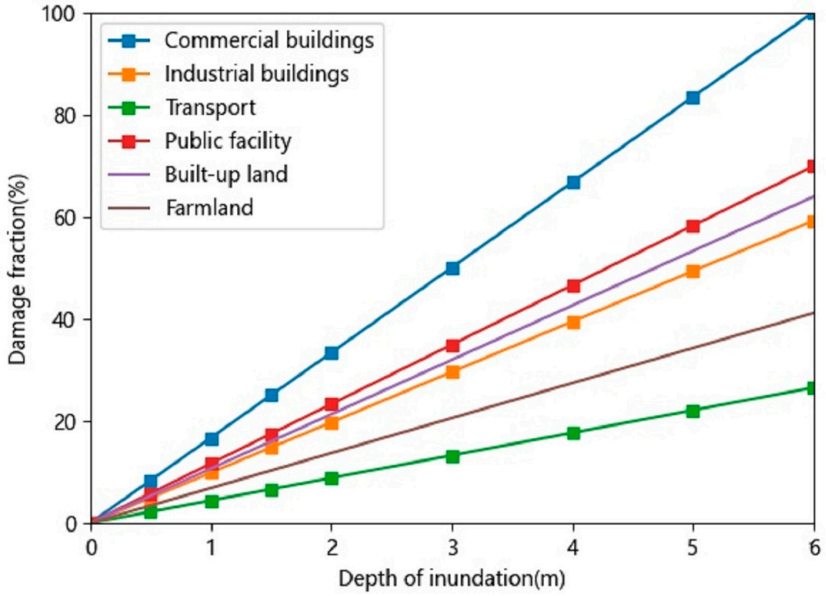

Figure 3. Vulnerability curves for various land types.

3.2.2. Flood Inundation Analysis

Based on LULC, as well as future LULC simulations, this study employs a simplified hydrodynamic to simulate flood inundation scenarios under different return periods. This study primarily focused on pluvial floods, considering the severity of this type of flood in the study area. As a driving force of pluvial floods, precipitation information was used as the main input for flood hazards analysis. Based on the trend analysis of precipitation in recent years, it was found that the precipitation in Chongqing shows fluctuations, with weak upward trends [57]. Therefore, we decided that the rainfall in the near future (i.e., 2030) is likely to be in an "unchanged" state. To balance the accurate computational costs, 24 h rainfall was applied to simulate the flooding processes.

A simplified 2D flood inundation model (FloodMap-Inertial [43])—a revised version of an earlier diffusion-based model [40,41]—was used to simulate pluvial floods. The model integrates hydrological processes (e.g., infiltration, evapotranspiration, and drainage). Studies have shown that advection has a small effect on the shallow-water equation and can be ignored [38]. The models are discretized in both space and time. This discretization is raster-based and solves the inertial form of the 2D shallow water equations [40,41]. Flood routing takes the same form as the inertial algorithm created by Bates et al. (2010), but with a slightly different method for calculating the time steps, while the time step is variable and is forward calculated for each iteration. On this basis, the equations are discretized in terms of time steps Δt, which then forward calculate the optimal time step for the next

iteration. The details of the model are described by Yu and Coulthard [43]. Therefore, we only focus on the major features of the model, in which the discrete form was given by:

$$q_{t+\Delta t} = \frac{q_t - gh_t\Delta t(\frac{\Delta(h_t+z)}{\Delta x})}{(1 + gh_t\Delta tn^2q_t/h_t^{10/3})} \quad (6)$$

where q is the flow per unit width, g is the acceleration due to gravity, z is the bed elevation, h is the water depth, and n is the Manning's roughness coefficient. With reference to a previous study, roughness is represented in this model by the floodplain Manning coefficient n. The n values for urban areas, cropland, green land (woodland and grassland), water bodies, and bare land are assigned values of 0.01, 0.06, 0.08, 0.03, and 0.035, respectively [58].

In this study, we first inputted various datasets into the model, including a digital elevation model (DEM), historical precipitation distributions across different return periods, and Manning's coefficient maps. Subsequently, we meticulously adjusted and calibrated the model parameters, ensuring that they were consistent with the specific requirements of our research. Considering that the Forward Courant–Friedrichs–Lewy Condition (FCFL) might not always provide the most suitable stability criterion for inertial systems, we adjusted the determined time step by applying a scaling coefficient within the range of (0, 1]. Previous studies found stability in a scaling factor range of 0.5–0.8, with this study using a scaling factor of 0.7 for all simulations [59]. Given the focus of the present study, a 30 m resolution simulation was regarded as a legitimate trade-off between computational demand and simulation detail. The infiltration over saturation is determined by the widely used Green–Ampt equation. Hydraulic conductivity (Ks) is a key parameter for infiltration. The value of hydraulic conductivity between 0.001 m/h and 0.003 m/h showed a good fit [43]. We have conducted a sensitivity analysis on the selection of this value, as detailed in the Supplementary Materials—Figure S1. Considering that the study concerns urbanization, a hydraulic conductivity value of 0.001 m/h was adopted for the remaining simulations. We assumed an evapotranspiration of 3 mm d^{-1}, a value that generates a good inundation prediction for hydro-inundation modeling. Empirically based correlation methods or in situ hydraulic laboratory measurements can be used to determine the value of Ks. Since Chongqing is located in a rural area, we did not consider the urban drainage capacity in this simulation.

Although the study area is prone to pluvial floods, there are few aerial images or field surveys of the floods in this area. Thus, 29 flood-prone points were collected from the Chongqing media as verification points. The details for verifying these points are attached in Table S1. Considering that the precipitation in 2-year flood events is above 100 mm, the flood-prone points were used to verify the simulation of flood events [60]. Moreover, flood-prone points are described briefly, and it is difficult to geo-locate them at a 30 m resolution. If the simulated inundation depth exceeds 30 cm within 300 m around the flood-prone point, the simulation is considered to reflect the actual distribution of the floods, and the validation case is defined as "1". Otherwise, the simulated flood area cannot reflect the actual flood distribution, and the validation case is defined as "0". As shown in Figure 4, the red points represent "1", while the black points represent "0". Among the 29 inundation points, 27 points have a validation condition of "1", which reflects a validation accuracy of 93.10%. The results show that the simulation of pluvial floods is feasible, to a certain extent.

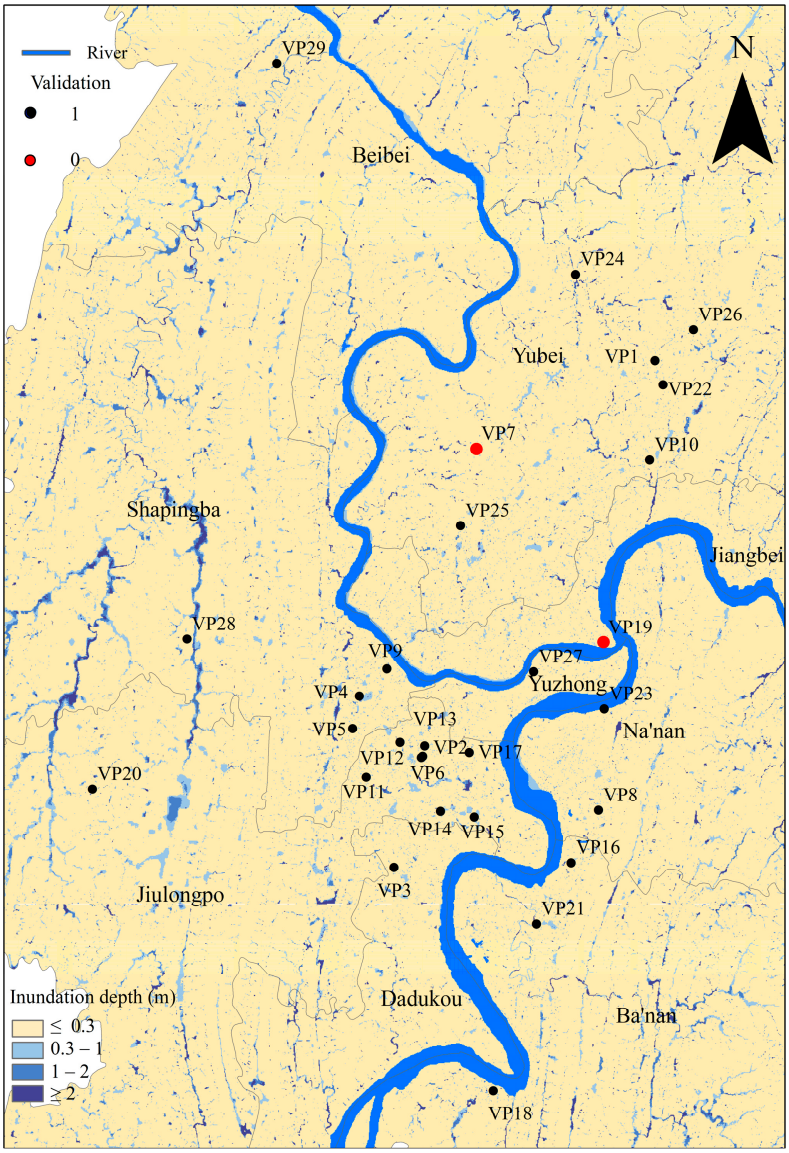

Figure 4. Accuracy validation points in the study area for the 2-year return period in 2018.

3.2.3. Flood Risk Assessment

Flood risk assessment generally includes the estimation of direct or indirect damages, e.g., the impact on the natural system, physical damage to buildings and infrastructure, loss of life, and disruptions to the economy [61]. This study focuses on direct flood damages for built-up land (including building structures, indoor properties, urban roads, and electrical facilities) and cropland. We use the hazard–vulnerability–exposure model to calculate the direct flood damages. Flood damage is estimated according to the following equation [62]:

$$D_j = (\sum_{i=1}^{n} x_i \times f(x_i)) \times A \quad (7)$$

where D_j is the flood damage (in USD million, as of 2011) over j return period of inundation, x_i is the depth of inundation (m) in cell i, $f(x_i)$ is the damage function (vulnerability and exposure) for the level of inundation depth x, and A is the area of a cell.

Multiplying the exposures by their individual vulnerability curves allowed us to calculate the economic losses in different return periods (2 years, 10 years, 20 years, 50 years, 100 years) for the four scenarios of 2010, 2015, 2018, and 2030. Therefore, the losses–exceedance probability curve is estimated using the economic losses and exceedance

probabilities of different flood events. In this study, the value of EAD is calculated to represent the risk of pluvial floods in a given year.

4. Results

4.1. The Temporal and Spatial Changes in LULC

Based on the LULC in 2010 and 2015, we obtained the land-use transfer area matrix (Table 1). The Markov chain model was used to estimate the transition probability for 2030. The built-up and cropland areas experienced dramatic changes, followed by the woodlands, while the watershed and bare land areas exhibited less significant changes. The area of cropland was greatly reduced by 126.8 km^2, and was mainly converted to built-up land. With the process of urbanization, the built-up land area rapidly increased to 130.8 km^2. The change in other land-use areas was relatively small. Comparing the predicted LULC map with the observed data from 2018, the validation process yielded a Kappa coefficient of 0.92, which indicates an acceptable degree of accuracy.

Table 1. Transfer area of land use matrix in Chongqing from 2010 to 2015 (km^2).

	Cropland	Woodland	Grassland	Water	Built-Up Land	Bare Land	Transfer Out
Cropland	3513.6	7.7	0.6	1.2	129.0	0.0	138.6
Woodland	7.8	1059.2	0.1	0.1	4.6	0.0	12.6
Grassland	0.6	0.1	48.6	0.3	0.2	0.0	1.1
Water	0.8	0.1	0.0	153.6	0.4	0.0	1.4
Built-up land	2.5	0.5	0.0	0.2	530.0	0.0	3.3
Bare land	0.0	0.0	0.0	0.0	0.0	2.8	0.0
Transfer in	11.8	8.5	0.7	2.0	134.1	0.0	157.0
Net transfer out	126.8	4.1	0.5	−0.6	−130.8	0.0	0

Note: 2010 is the base year of change, 2015 is the target year of change; rows indicate transfers out, and columns indicate transfers in.

We predict the LULC for 2030 based on the CA-Markov model. The LULC changes from 2010 to 2030 are shown in Figure 5. The area covered by cropland is the largest, followed by woodland, with water and bare land covering the smallest areas. This indicates that the landscape structure of the study area is dominated by agricultural and forestry production, which is consistent with the industrial structure of this region. Built-up land is mainly distributed in the Yuzhong District and its surrounding regions. Croplands are widely distributed, mainly in the hills and along rivers, with low elevations. Woodlands in these regions are relatively poorly exploited and well preserved at high altitudes owing to the complex topography and proper protection. Grasslands are mostly distributed in the eastern portion of the study area, where they are small and scattered. Water and bare land are less widely distributed. From 2010 to 2030, the cropland area shows little fluctuation, while the woodland area shows a continuous increase. With rapid urbanization, the area of built-up land continues to grow. The changes in water and bare land are ignored because of their smaller area. From 2010 to 2030, the area of built-up land experienced the largest rate of increase among the six LULC types. Built-up land is predicted to increase from 533.36 km^2 to 1377.79 km^2 from 2010 to 2030. The increasing built-up land area is mostly spread across Yuzhong District and its surrounding districts. Croplands show a decreasing trend. The cropland decreased from 66.83% in 2010 to 54.41% in 2030, a decrease of 18.59%. The area of cropland is mainly reduced around the surrounding built-up land in the 2018–2030 period. The areas of grassland and woodland increased during 2010–2015, but decreased during 2015–2018. We predict that the areas of grassland and woodland will decrease during the period of 2018–2030. The changed areas of grassland and woodland are located along mountains and hills.

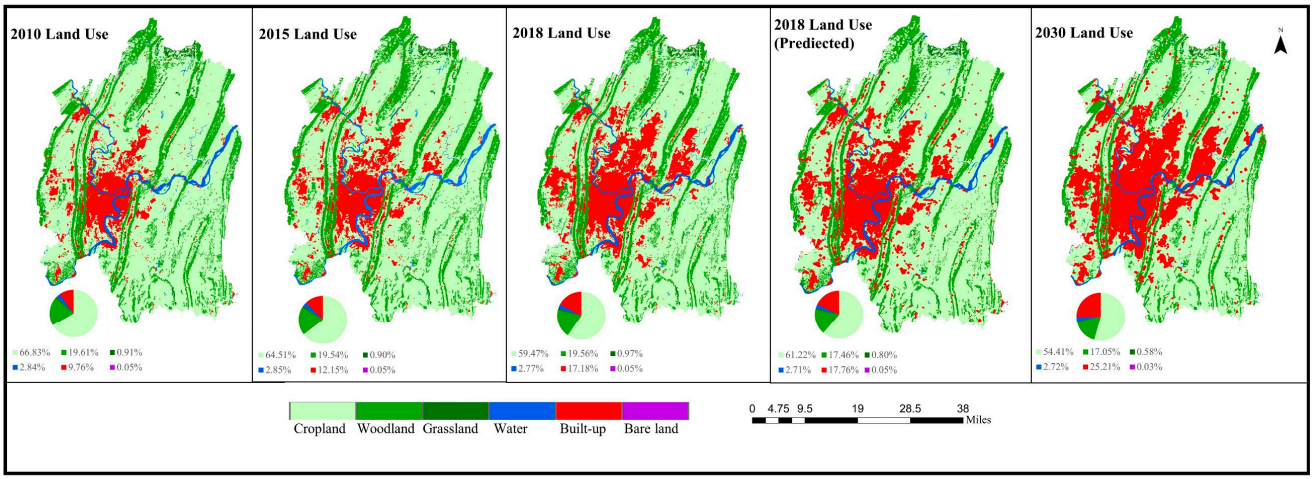

Figure 5. Land uses from 2010 to 2030.

The general dynamic attitude in Chongqing is indicated in Table 2. Built-up land shows the largest dynamic attitude, at 13.77% in 2018. The area of built-up land increased faster in 2015–2018 than in other periods. The grassland area decreased in 2010–2015 and 2018–2030 and increased in 2015–2018, with a fast growth rate. The dynamic attitude of woodlands shows the same trends, but the growth rate is slower than that of grasslands. The dynamic attitude of cropland is decreasing overall, and is relatively small during the 2010–2015 and 2018–2030 periods.

Table 2. Land-use change in Chongqing from 2010 to 2030.

		Cropland	Woodland	Grassland	Water	Built-Up Land	Bare Land
2010–2015	Change of area (km^2)	−126.77	−4.13	−0.50	0.58	130.83	−0.01
	Dynamic attitude/%	−0.69%	−0.08%	−0.20%	0.08%	4.91%	−0.09%
2015–2018	Change of area (km^2)	−275.35	1.09	4.06	−4.28	274.45	0.02
	Dynamic attitude/%	−2.60%	0.03%	2.75%	−0.92%	13.77%	0.19%
2018–2030	Change of area (km^2)	−276.74	−136.86	−21.91	−2.56	439.16	−1.07
	Dynamic attitude/%	−0.71%	−1.07%	−3.42%	−0.14%	3.90%	−3.15%

4.2. The Impacts of Urbanization Changes on Flood Risk

4.2.1. Flood Damage

Based on the analysis of the exceedance probability of 24 h of rainfall, the return periods of 2-year, 10-year, 20-year, 50-year, and 100-year events are selected as flood hazard scenarios. We simulated the inundation of floods for 2010, 2015, 2018, and 2030, with different return periods. We used 2018 as the case for analysis to show the cumulative density functions of the maximum inundation area (depth > 0.3 m) and average inundation depth for each return period, as shown in Figure 6. The inundation area and average depth are evidenced by a significant positive correlation with rainfall intensity. The maximum flood inundation area is 339.97 km^2, and the average inundation depth is 0.113 m under a 2-year return period event. With the increase in precipitation, the maximum inundation area increases by 61.67% and 67.08% for the 50-year and 100-year flood events, respectively. Similarly, the average water depth will increase by 0.098 m (86.73%) and 0.12 m (106.19%) for the 50-year and 100-year flood events, compared to the 2-year return period event. The inundation area and depth are evidenced by the significant positive correlation with rainfall intensity, which is in accordance with the results of previous studies. In the inundation area, cropland and built-up land are the major land-use types. This indicates that the urban socioeconomic system would experience large impacts from pluvial floods.

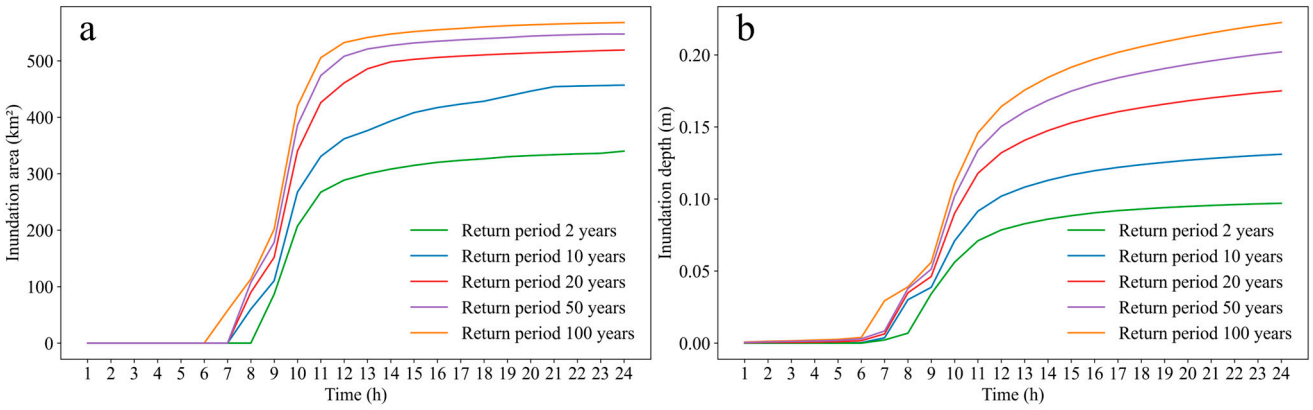

Figure 6. The simulated inundation maximum area (**a**) and average depth (**b**) with different return periods for 2018.

In Figure 7, we show a comprehensive representation of the hydrological response in 2018, with a 100-year return period, by illustrating the progression of infiltration loss, the distribution of rainfall, and the flood inundation patterns. For the rainfall in 0–7 h, the flood inundation area and average depth remained relatively stable. The infiltration loss begins at a relatively moderate rate. This could be attributed to the lack of penetration of the initial rainfall or its adequate flow into adjacent bodies of water. For the precipitation in 7–11 h, there was a significant increase in rainfall, causing more water to enter the watershed, as showed in Figure 7b. After the initial 11 h of rainfall, the increase in the flood inundation area and the depth slowed down. The incremental increase in loss is more linear, suggesting a stabilization of the infiltration process. By 16 h, the infiltration loss reaches 184.01 $\times$ 107 m^3, after which the rate of increase further moderates, as shown in Figure 7b. Figure 7 indicates that the depth of flood inundation further increased during the last 8 h of rainfall, as previous moisture was still flowing into the bodies of water, and surface runoff continued.

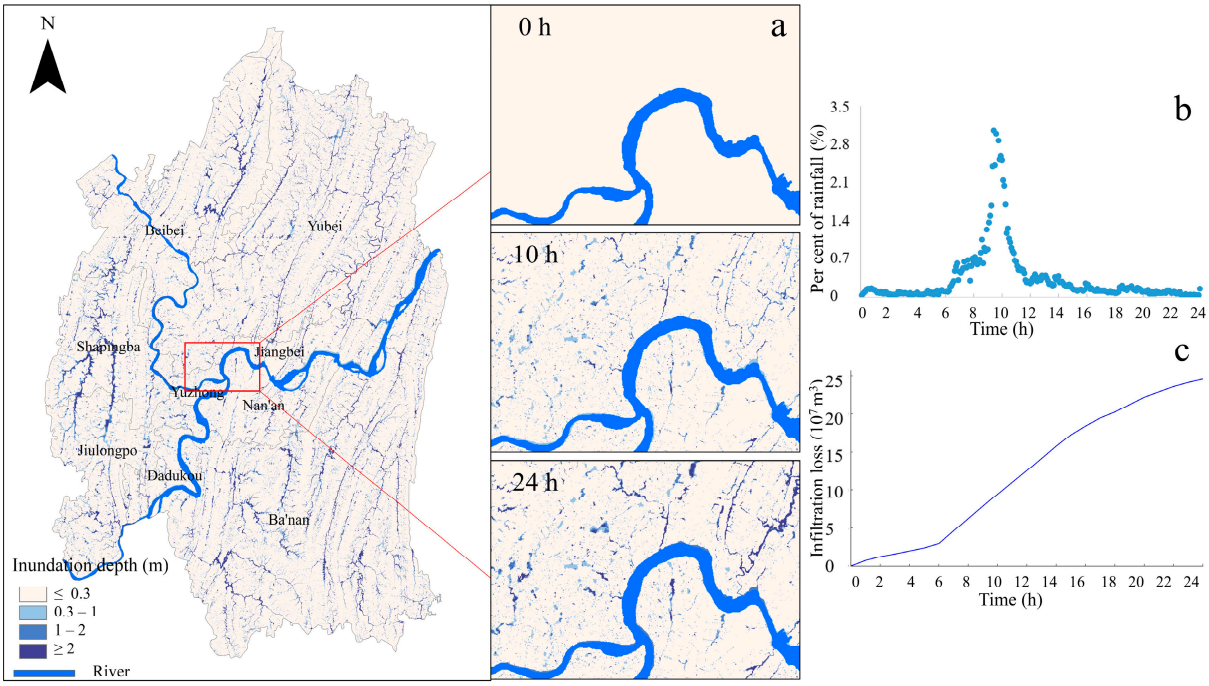

Figure 7. The simulated maximum inundation maps at different time intervals for 2018, showing the 100-year return period (**a**), rainfall distribution (**b**), and infiltration loss (**c**).

To further explore the impacts of urbanization on inundation mitigation, we simulated inundation in 2010, 2015, 2018, and 2030 under different LULC scenarios. We set four hazard levels in regards to inundation depth (ID): high (>2 m), medium (1–2 m), low (0.3–1 m), and very low (<0.3 m), based on the literature and observed data for the study area (Table 3). The area with a very low ID shows a steady increase over time, which more than tripled from 2010 to 2030. In comparison, the changes in low, medium, and high ID are dramatic, with a much higher rate of change during the study period. With an increase in the inundation depth (or level), the growth rate of the inundated area increased. The area with a low ID for 2010 is predicted to be 32.69 km^2, which may increase more than nine times (301.61 km^2) by 2030. The area of medium inundation depth will increase 10 times from 2010 to 2030, and the area with a high ID in 2030 will increase 16 times compared to that in 2010. In terms of inundation area, there is one phase of rapid growth between 2015 and 2018. During this period, the built-up land experienced rapid expansion. Urbanization is typically accompanied by changes in land use, including the expansion of roads, buildings, and other impervious surfaces, leading to dynamic alterations in the watershed. Urbanization results in an increase in impervious surfaces. These surfaces prevent rainwater from infiltrating the soil, rapidly directing it into drainage systems and thereby increasing the depth of flood inundation. Consequently, urban planning and management must consider strategies to reduce the coverage of impervious surfaces to aid in the mitigation of flood risks.

Table 3. Flood inundation area with 50-year return periods.

ID	2010 (km^2)	2015 (km^2)	2018 (km^2)	2030 (km^2)
Very low	474.52	595.49	838.16	1228.11
Low	32.68	37.30	50.46	301.61
Medium	14.0	16.40	24.01	147.23
High	11.96	14.80	25.80	178.21

4.2.2. Flood Risk

By calculating the distribution of flood hazards, vulnerability, and land value, we can examine the direct economic losses. Figure 8 shows the flood damage, with different return periods, for 2010, 2015, 2018, and 2030. Flood damage has a tendency to increase significantly as the return period increases. The damage is estimated to increase approximately 2.5 times with return periods from 2 to 100 years. The calculation of EAD typically involves estimating losses under multiple flood scenarios, then summing the present value of these losses and dividing this by a certain period to obtain an annual average. This method provides a uniform comparison of losses at different points in time, presenting a more comparable metric. The EAD in 2010 is estimated to be approximately USD 68.07 million, a figure which may more than triple (USD 200.91 million) by the year 2030. Flood risk is a function of hazard, vulnerability, and land value. The expansion of built-up land use has resulted in an upward trend regarding flood vulnerability and exposure. This is consistent with previous studies that reported an important role of urbanization in flood risk in several regions around the world. For instance, Zhang et al. [63] quantified the contribution of urbanization to floods and found that the probability of such floods increased approximately 21 times owing to the urbanization of Houston, United States. This paper quantifies the impact of urbanization on flood risk in Chongqing, emphasizing the need for the comprehensive consideration of flood risks during urban planning to ensure the sustainable development of the city [17].

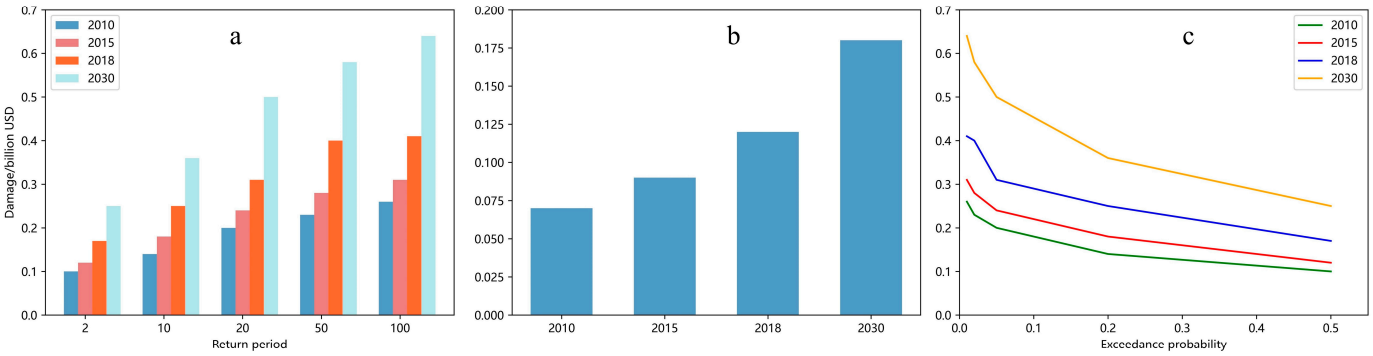

Figure 8. (**a**) Estimated damages from different return periods in 2010, 2015, 2018, and 2030; (**b**) comparison of EAD in 2010, 2015, 2018, and 2030; (**c**) probability of exceeding the distribution curve.

4.2.3. The Association of Flood Risk Factors Analysis

In this study, we aim to investigate the association between flood risk and natural and socioeconomic factors at a fine spatial scale using Spearman's rank coefficient. Shi et al. [64] developed a comprehensive poverty index (CPI) dataset for Chongqing using multi-data from 2018. In this study, we consider CPI, which is typically used to measure social and economic development within a specific population and area, as a socioeconomic index (SEI). Higher values of the index indicate a more prosperous economy in a region.

In this study, 1000 random sample points were created using the Create Random Points tool in ArcMap. These points were used to extract the spatial environment parameters for 2018. The environmental parameters, including SEI, slope, elevation, LULC, and population density, were selected based on their roles in influencing flood risk, and they are available as gridded data. Table 4 summarizes the results of the correlation analysis used to explain the influence of different parameters on flood risk. The results show that flood risk is relatively higher in areas with a high population density. Areas with high population density are generally more susceptible to the impact of floods, as a greater number of people may reside in potential flood-prone zones. Additionally, high population density can lead to increased demand for infrastructure, thereby amplifying the potential losses caused by floods [65]. LULC also exhibits a significant correlation with flood risk. A similar pattern of association has been reported in other regions [66]. Different land uses and land cover types produce varying impacts on flood risk. Urbanization and human development can lead to an increase in impermeable surfaces, thereby increasing surface runoff and elevating flood risk. Conversely, natural vegetation and wetlands may contribute to lowering flood risk, as they help slow down water flow and facilitate the absorption of moisture [16,18]. However, the SEI, DEM, and slope are negatively correlated with flood risk in Chongqing. In summary, the slope is more correlated with flood risk than are the other factors. This can be attributed to the influence of the natural environment. Surface slope directly influences the direction of precipitation runoff and the formation of drainage basins. Steeper slopes can result in faster water flow, increasing the speed of flood initiation and propagation. Therefore, areas with a greater slope are generally more susceptible to the impact of flooding [67]. A higher elevation and slope will greatly increase the cost of constructing infrastructure, implying a lower level of human exposure in the area. SEI is a commonly used indicator of the level of socioeconomic development in Chongqing. Wang et al. showed that the urbanization rate and GDP per capita are positively correlated with flood risk [68]. Li et al. reported that higher-income countries may possess higher standards of flood protection and stronger flood mitigation capacities, which may reduce flood damage [69].

Table 4. The analysis of the association of flood risk factors.

	Flood Risk
SEI	−0.057 *
LULC	0.095 **
Population-density	0.049 **
DEM	−0.097 **
Slope	−0.112 **

Significance level: ** 0.01; * 0.05.

5. Discussion

This study analyzed and simulated the changes in LULC, based on historical trends for flood risk assessment. The results are similar to those from other studies in terms of the expansion of built-up land and the decrease in cropland [70]. For example, the study by Zuo et al. also revealed a considerable shift in land use in Chongqing from 2000 to 2020, with woodland, water area, and built-up land expanding greatly, while cropland and grassland decreased [71]. However, while simulating future LULC is subject to uncertainty, our study provides a comprehensive analysis of LULC changes. Due to a lack of spatial data, our study was unable to investigate several potential socioeconomic factors, including variables like agricultural productivity, land-use policies, changes in transportation infrastructure, and individual preferences [15,72,73]. In addition, more sophisticated models can be developed in the future to simulate urban growth in different areas of the study region.

We found that the pluvial floods that occur each year cause substantial damage in Yuzhong District. The flood damage is attributed to the geomorphological characteristics and socioeconomic status of the study area. Urban areas with a higher level of prosperity tend to be located at lower elevations and slopes in the mountainous region. Naturally, a lower slope and lower elevation are assigned to the highest rank of risk, i.e., they are more susceptible to flood hazards. Reported data on historical flood losses are scarce in the study area, particularly for pluvial floods. Therefore, it is difficult to verify our results. Regarding flooding in Chongqing, the Yearbook of Meteorological Disasters in China (2011) reported total economic losses of USD 819.39 million in 2010. In addition, local heavy precipitation usually triggers secondary disasters such as flash floods, transit floods, and landslides. Such secondary disasters were not included in our work. Thus, the losses resulting from flood events are estimated to be much lower than those reported for several previous occurrences. Therefore, future studies should integrate additional drivers and impact factors into city-level flood risk assessment, determining their relative contributions in order to provide accurate information for decision making in regards to adaptation.

However, the performance of the modeling result is inevitably affected by data limitations and the assumptions and simplifications of the methodology. The quality of the input data also contributes to the accuracy of the model predictions. Rainfall distribution is expected to be an important factor to consider. In this study, we chose a fixed value for rainfall, but in reality, rainfall is unevenly distributed. Consequently, we may overestimate or underestimate flood risks in certain areas, even though the dataset's reliability is reinforced by its origin from a respected government institution. Hence, adopting a more precise representation of rainfall could enhance predictions for specific localities. Many existing studies have already investigated the impact of spatial rainfall patterns on hydrological predictions, including the employment of comparisons with the use of weather radar data [74]. Future research could further explore this aspect. It is very difficult to create accurate near-future forecasts of large-scale changes in spatiotemporal precipitation. Our assumption of "unchanged" rainfall in the near future was generated due to the inherent difficulties in forecasting such changes. In the event that future precipitation levels, particularly for 24 h events, exceed the baseline values, this could lead to an underestimation of flood risk, underlining the need for ongoing monitoring and the adjustment of our flood risk assessments as new data and forecasting capabilities become available. Another source of input data uncertainty is related to the DEM. Urban topog-

raphy can be complex due to the presence of manmade structures. While the 30 m DEM used in our study effectively captured the primary topographic characteristics of the study area, it may not have adequately represented the intricacies of local topography. This is particularly relevant in urban settings, where fine-scale variations in elevation caused by man-made structures can significantly influence flood patterns. For future research, employing higher-resolution DEMs could address this limitation by providing a more detailed representation of urban topography and improving the accuracy of flood risk assessments. The collected flood-prone points exhibit uncertainties in both their spatial and temporal attributes. Spatial uncertainties primarily stem from the lack of precise geospatial data, while temporal uncertainties are associated with imprecise reporting times. Future research should prioritize the establishment of more monitoring sites and the enhancement of temporal resolution for more robust data collection.

In addition, EAD estimates are subject to great uncertainty originating from various sources, including hydrological and hydraulic modeling, the application of damage curves (relating water depth to damage rate), and the EAD estimation approach itself. Comprehensive uncertainty analysis must account for these sources of error in the estimation model and measure its sensitivity to changes in input variables and internal parameters, as well as quantify the contribution of each source of uncertainty to the overall error. Despite its importance, this issue is beyond the scope of the present study. Socioeconomics is generally considered to be an indicator of the flood vulnerability index or flood risk [75]. The relationship between floods and the socioeconomic index is usually analyzed in administrative units at country or regional (province or county) levels [68]. This study further presents a correlation analysis to estimate the flood risk at local scales. It is widely recognized that an increase in flood risk may restrict the development of socioeconomic conditions and inhibit long-term sustainable development [76]. Individuals on a low income tend to live in marginal and flood-prone areas, where floods trap people in a cycle of poverty [77]. In reality, the relationship between flood risk and socioeconomic factors is complex. Various factors influence flood risk, such as climate change, urbanization, infrastructure, and the level of emergency management. In the future, we should explore the mechanisms underlying the impact of the interaction of multiple factors on flood risk.

6. Conclusions

This study proposes an integrated approach based on remote sensing data to effectively assess flood risk under urbanization at a city scale. This approach integrates CA-Markov, simplified hydrodynamic models, and damage models, implementing them in Chongqing, China. The spatiotemporal distribution of flood risk at a city scale, along with its influencing factors, are illustrated in this study. From 2010 to 2030, cropland makes up the largest area, followed by woodland. During this period, the area covered by cropland is greatly reduced by 126.8 km^2 and is mainly converted to built-up land. In general, the dynamic attitude in Chongqing showed a decreasing trend for cropland, bare land, and grassland. In 2018, built-up land exhibited the largest dynamic attitude at 13.77%. With the increase in precipitation in 2018, the maximum inundation area and depth significantly increased by 67.08% and 106.19% for the 100-year flood events compared to the 2-year flood events, respectively. The area with a high ID is predicted to increase from 11.96 km^2 in 2010 to 178.21 km^2 in 2030. The growth rate of areas with high ID is higher than that of the very low, low, and medium ID areas. The damage is estimated to increase approximately 2.5 times, with return periods from 2 to 100 years. The EAD of USD 68.07 million in 2010 is predicted to increase significantly to USD 200.91 million in 2030. Our results show that a lower flood risk is found in areas with a smaller population or with higher socioeconomic development. The proposed approach for assessing the implications of flood risk under urbanization can be used as a reference for city scale flood risk mapping, particularly for the development of flood mitigation measures and emergency management strategies.

Supplementary Materials: The following supporting information can be downloaded at: https://www.mdpi.com/article/10.3390/rs16020219/s1, Table S1: Description of validation points; Figure S1: Sensitivity analysis of hydraulic conductivity. Reference [43] is cited in the supplementary materials.

Author Contributions: Conceptualization, Y.L. and S.W.; data curation, Y.L., J.G. and S.W.; formal analysis, Y.L., J.G. and S.W.; methodology, J.Y. and Y.L.; writing—original draft, Y.L.; writing—review and editing, Y.L., L.L. and C.Z.; visualization, Y.L.; supervision, J.Y., J.G. and S.W.; project administration, J.G. and S.W.; funding acquisition, S.W. All authors have read and agreed to the published version of the manuscript.

Funding: This research was funded by the National Natural Science Foundation of China (42271089, 42101311, 42371084).

Data Availability Statement: Data are available on request from the authors.

Acknowledgments: We gratefully acknowledge the anonymous reviewers and the editors for their comments and suggestions that improved this manuscript.

Conflicts of Interest: The authors declare no conflicts of interest.

References

1. IPCC. *Climate Change 2021: The Physical Science Basis. Contribution of Working Group I to the Sixth Assessment Report of the Intergovernmental Panel on Climate Change*; Cambridge University Press: Cambridge, UK; New York, NY, USA, 2021; p. 2391.
2. Marsooli, R.; Lin, N.; Emanuel, K.; Feng, K. Climate change exacerbates hurricane flood hazards along US Atlantic and Gulf Coasts in spatially varying patterns. *Nat. Commun.* **2019**, *10*, 3785. [CrossRef] [PubMed]
3. United Nations Office for Disaster Risk Reduction (UNISDR) & Centre for Research on the Epidemiology of Disasters (CRED). The Human Cost of Natural Disasters: A Global Perspective. Available online: https://reliefweb.int/report/world/human-cost-natural-disasters-2015-global-perspective (accessed on 22 May 2022).
4. He, B.; Huang, X.; Ma, M.; Chang, Q.; Tu, Y.; Li, Q.; Zhang, K.; Hong, Y. Analysis of flash flood disaster characteristics in China from 2011 to 2015. *Nat. Hazards* **2018**, *90*, 407–420. [CrossRef]
5. EM-DAT. The OFDA/CRED International Disaster Database. Available online: https://www.emdat.be/ (accessed on 22 May 2022).
6. Xiao, Y.; Yi, S.; Tang, Z. A Spatially Explicit Multi-Criteria Analysis Method on Solving Spatial Heterogeneity Problems for Flood Hazard Assessment. *Water Resour. Manag.* **2018**, *32*, 3317–3335. [CrossRef]
7. Deng, Z.; Wang, Z.; Wu, X.; Lai, C.; Zeng, Z. Strengthened tropical cyclones and higher flood risk under compound effect of climate change and urbanization across China's Greater Bay Area. *Urban Clim.* **2022**, *44*, 101224. [CrossRef]
8. Zhao, J.; Chen, H.; Liang, Q.; Xia, X.; Xu, J.; Hoey, T.; Barrett, B.; Renaud, F.G.; Bosher, L.; Zhou, X. Large-scale flood risk assessment under different development strategies: The Luanhe River Basin in China. *Sustain. Sci.* **2022**, *17*, 1365–1384. [CrossRef]
9. Guoyi, L.; Liu, J.; Shao, W. Urban flood risk assessment under rapid urbanization in Zhengzhou City, China. *Reg. Sustain.* **2023**, *4*, 332–348. [CrossRef]
10. Yu, I.; Jung, H. Flood Risk Assessment to Enable Improved Decision-Making for Climate Change Adaptation Strategies by Central and Local Governments. *Sustainability* **2022**, *14*, 14335. [CrossRef]
11. Baky, M.A.A.; Islam, M.; Paul, S. Flood Hazard, Vulnerability and Risk Assessment for Different Land Use Classes Using a Flow Model. *Earth Syst. Environ.* **2020**, *4*, 225–244. [CrossRef]
12. Schwarz, I.; Kuleshov, Y. Flood Vulnerability Assessment and Mapping: A Case Study for Australia’s Hawkesbury-Nepean Catchment. *Remote Sens.* **2022**, *14*, 4894.
13. Wu, S.; Liu, L.; Gao, J.; Wang, W. Integrate Risk From Climate Change in China Under Global Warming of 1.5 and 2.0 °C. *Earth's Future* **2019**, *7*, 1307–1322. [CrossRef]
14. Koks, E.E.; Jongman, B.; Husby, T.G.; Botzen, W.J.W. Combining hazard, exposure and social vulnerability to provide lessons for flood risk management. *Environ. Sci. Policy* **2015**, *47*, 42–52. [CrossRef]
15. Güneralp, B.; Güneralp, İ.; Liu, Y. Changing global patterns of urban exposure to flood and drought hazards. *Glob. Environ. Chang.* **2015**, *31*, 217–225. [CrossRef]
16. Garg, V.; Aggarwal, S.; Gupta, P.K.; Nikam, B.R.; Thakur, P.K.; Srivastav, S.; Senthil Kumar, A. Assessment of land use land cover change impact on hydrological regime of a basin. *Environ. Earth Sci.* **2017**, *76*, 635. [CrossRef]
17. Hemmati, M.; Ellingwood, B.R.; Mahmoud, H.N. The role of urban growth in resilience of communities under flood risk. *Earth's Future* **2020**, *8*, e2019EF001382. [CrossRef] [PubMed]
18. Mandarino, A.; Faccini, F.; Luino, F.; Bono, B.; Turconi, L. Integrated Approach for the Study of Urban Expansion and River Floods Aimed at Hydrogeomorphic Risk Reduction. *Remote Sens.* **2023**, *15*, 4158. [CrossRef]
19. Cai, J.; Li, X.; Liu, L.; Chen, Y.; Wang, X.; Lu, S. Coupling and coordinated development of new urbanization and agro-ecological environment in China. *Sci. Total Environ.* **2021**, *776*, 145837. [CrossRef]

20. Mechler, R.; Bouwer, L.M.; Linnerooth-Bayer, J.; Hochrainer-Stigler, S.; Aerts, J.C.; Surminski, S.; Williges, K. Managing unnatural disaster risk from climate extremes. *Nat. Clim. Chang.* **2014**, *4*, 235–237. [CrossRef]
21. Broderick, C.; Murphy, C.; Wilby, R.L.; Matthews, T.; Prudhomme, C.; Adamson, M. Using a scenario-neutral framework to avoid potential maladaptation to future flood risk. *Water Resour. Res.* **2019**, *55*, 1079–1104. [CrossRef]
22. Zhou, Q.; Leng, G.; Su, J.; Ren, Y. Comparison of urbanization and climate change impacts on urban flood volumes: Importance of urban planning and drainage adaptation. *Sci. Total Environ.* **2019**, *658*, 24–33. [CrossRef]
23. Xu, H.; Tian, Z.; Sun, L.; Ye, Q.; Ragno, E.; Bricker, J.; Mao, G.; Tan, J.; Wang, J.; Ke, Q. Compound flood impact of water level and rainfall during tropical cyclone periods in a coastal city: The case of Shanghai. *Nat. Hazards Earth Syst.* **2022**, *22*, 2347–2358. [CrossRef]
24. Dada, O.A.; Almar, R.; Morand, P.; Bergsma, E.W.J.; Angnuureng, D.B.; Minderhoud, P.S.J. Future socioeconomic development along the West African coast forms a larger hazard than sea level rise. *Commun. Earth Environ.* **2023**, *4*, 150. [CrossRef]
25. Tang, J.; Li, W.; Fang, J.; Zhang, Z.; Du, S.; Wu, Y.; Wen, J. Scenario-based economic and societal risk assessment of storm flooding in Shanghai. *Int. J. Clim. Chang. Strat. Manag.* **2021**, *13*, 529–546. [CrossRef]
26. Kang, S.; Yin, J.; Gu, L.; Yang, Y.; Liu, D.; Slater, L. Observation-Constrained Projection of Flood Risks and Socioeconomic Exposure in China. *Earth's Future* **2023**, *11*, e2022EF003308. [CrossRef]
27. Zhou, N.; Sheng, S.; He, L.-Y.; Tian, B.-R.; Chen, H.; Xu, C.-Y. An Integrated Approach for Analyzing the Morphological Evolution of the Lower Reaches of the Minjiang River Based on Long-Term Remote Sensing Data. *Remote Sens.* **2023**, *15*, 3093. [CrossRef]
28. Huang, W.; Liu, H.; Luan, Q.; Jiang, Q.; Liu, J.; Liu, H. Detection and prediction of land use change in Beijing based on remote sensing and GIS. *Int. Arch. Photogramm. Remote Sens. Spat. Inf. Sci.* **2008**, *37*, 75–82.
29. Lin, W.; Sun, Y.; Nijhuis, S.; Wang, Z. Scenario-based flood risk assessment for urbanizing deltas using future land-use simulation (FLUS): Guangzhou Metropolitan Area as a case study. *Sci. Total Environ.* **2020**, *739*, 139899. [CrossRef] [PubMed]
30. Muis, S.; Güneralp, B.; Jongman, B.; Aerts, J.C.; Ward, P.J. Flood risk and adaptation strategies under climate change and urban expansion: A probabilistic analysis using global data. *Sci. Total Environ.* **2015**, *538*, 445–457. [CrossRef]
31. Mustafa, A.; Bruwier, M.; Archambeau, P.; Erpicum, S.; Pirotton, M.; Dewals, B.; Teller, J. Effects of spatial planning on future flood risks in urban environments. *J. Environ. Manag.* **2018**, *225*, 193–204. [CrossRef]
32. Sang, L.; Zhang, C.; Yang, J.; Zhu, D.; Yun, W. Simulation of land use spatial pattern of towns and villages based on CA–Markov model. *Math. Comput. Model.* **2011**, *54*, 938–943. [CrossRef]
33. Fu, X.; Wang, X.; Yang, Y.J. Deriving suitability factors for CA-Markov land use simulation model based on local historical data. *J. Environ. Manag.* **2018**, *206*, 10–19. [CrossRef]
34. Zhang, C.-X.; Xu, J.-J.; Wen, J.; Yang, X.-B.; Wang, J.; Zhao, B. Dynamic simulation of landscape change in the Baiyangdian basin based on the CA-Markov model and MCE constraints. *J. Agric. Resour. Environ.* **2021**, *38*, 655–664.
35. Kindu, M.; Schneider, T.; Döllerer, M.; Teketay, D.; Knoke, T. Scenario modelling of land use/land cover changes in Munessa-Shashemene landscape of the Ethiopian highlands. *Sci. Total Environ.* **2018**, *622–623*, 534–546. [CrossRef] [PubMed]
36. Nkwunonwo, U.C.; Whitworth, M.; Baily, B. A review of the current status of flood modelling for urban flood risk management in the developing countries. *Sci. Afr.* **2020**, *7*, e00269. [CrossRef]
37. Bulti, D.T.; Abebe, B.G. A review of flood modeling methods for urban pluvial flood application. *Model. Earth Syst. Environ.* **2020**, *6*, 1293–1302. [CrossRef]
38. Bates, P.D.; Horritt, M.S.; Fewtrell, T.J. A simple inertial formulation of the shallow water equations for efficient two-dimensional flood inundation modelling. *J. Hydrol.* **2010**, *387*, 33–45. [CrossRef]
39. Teng, J.; Jakeman, A.J.; Vaze, J.; Croke, B.F.; Dutta, D.; Kim, S. Flood inundation modelling: A review of methods, recent advances and uncertainty analysis. *Environ. Model. Softw.* **2017**, *90*, 201–216. [CrossRef]
40. Yu, D.; Lane, S.N. Urban fluvial flood modelling using a two-dimensional diffusion-wave treatment, part 2: Development of a sub-grid-scale treatment. *Hydrol. Process.* **2006**, *20*, 1567–1583. [CrossRef]
41. Yu, D.; Lane, S.N. Urban fluvial flood modelling using a two-dimensional diffusion-wave treatment, part 1: Mesh resolution effects. *Hydrol. Process.* **2006**, *20*, 1541–1565. [CrossRef]
42. Bradbrook, K. JFLOW: A multiscale two-dimensional dynamic flood model. *Water Environ. J.* **2006**, *20*, 79–86. [CrossRef]
43. Yu, D.; Coulthard, T.J. Evaluating the importance of catchment hydrological parameters for urban surface water flood modelling using a simple hydro-inundation model. *J. Hydrol.* **2015**, *524*, 385–400. [CrossRef]
44. Hawker, L.; Uhe, P.; Paulo, L.; Sosa, J.; Savage, J.; Sampson, C.; Neal, J. A 30 m global map of elevation with forests and buildings removed. *Environ. Res. Lett.* **2022**, *17*, 024016. [CrossRef]
45. Fu, Y.; Wang, Z. A Study of County's Economic Group Development Model in Chongqing. *Stud. Sociol. Sci.* **2015**, *6*, 63.
46. Li, Q.; Zheng, Y.; Zhou, G.; Zhu, Y.; Liu, C.; Liu, Y. Diurnal variations of rainfall affected by complex topography based on high-density observation in Chongqing over southwest China. *Theor. Appl. Climatol.* **2022**, *148*, 1373–1394. [CrossRef]
47. Qianzhu, Z.; Huoming, Z.; Yang, L.; Ruiyi, Z.; Qiang, G.; Jianmei, Y.; Kun, S. Research on chongqing mountain flood disaster risk assessment system based on AHP-GIS. In *IOP Conference Series: Earth and Environmental Science*; IOP Publishing: Bristol, UK, 2019; p. 032028.
48. Jiao, M.Y. *China Meteorological Disaster Yearbook*; China Meteorological Press: Beijing, China, 2019; pp. 86–157.

49. Chongqing Housing and Urban-Rural Development Commission. Information on the Publication of the Revised Formulae for Storm Intensity and the Design of Storm Rain Patterns in Chongqing. Available online: https://zfcxjw.cq.gov.cn/zwxx_166/gsgg/201708/t20170823_4216173.html (accessed on 10 August 2022).
50. Mansour, S.; Al-Belushi, M.; Al-Awadhi, T. Monitoring land use and land cover changes in the mountainous cities of Oman using GIS and CA-Markov modelling techniques. *Land Use Policy* **2020**, *91*, 104414. [CrossRef]
51. Liu, J.; Tian, Y.; Tian, L.; Zhang, X.; Wan, Z.; Liu, X. A Comparative Study on Planning Constraints of the Rapid Urbanization Area Expansion Simulation. *Geogr. Geo-Inform. Sci.* **2019**, *35*, 82–88.
52. Mondal, M.S.; Sharma, N.; Garg, P.K.; Kappas, M. Statistical independence test and validation of CA Markov land use land cover (LULC) prediction results. *Egypt. J. Remote Sens. Space Sci.* **2016**, *19*, 259–272. [CrossRef]
53. Yu, L.; Li, M.; Wang, S.; Zhao, Y. Wetland landscape change in Daliaohe River basin and the driving factors analysis. *Procedia Environ. Sci.* **2010**, *2*, 1255–1264. [CrossRef]
54. Yin, J. Study on the Risk Assessment of Typhoon Strom Tide in China Coastal Area. Ph.D. Thesis, East China Normal University, Shanghai, China, 2011.
55. Moel, H.; Huizinga, J.; Szewczyk, W. *Global Flood Depth-Damage Functions—Methodology and the Database with Guidelines*; European Commission, Joint Research Centre: Sevilla, Spain, 2016; pp. 35–56.
56. Feng, A. Change and Disaster Risk of Extreme Water Levels under Sea-Level Rise Scenarios in Coastal Region, Shandong. Ph.D. Thesis, Institute of Geographic Sciences and Natural Resources Research, Chinese Academy of Sciences, Beijing, China, 2017.
57. Liu, L.; Xu, Z.X. Regionalization of precipitation and the spatiotemporal distribution of extreme precipitation in southwestern China. *Nat. Hazards* **2016**, *80*, 1195–1211. [CrossRef]
58. Yin, J.; Yu, D.; Yin, Z.; Wang, J.; Xu, S. Modelling the anthropogenic impacts on fluvial flood risks in a coastal mega-city: A scenario-based case study in Shanghai, China. *Landsc. Urban Plan.* **2015**, *136*, 144–155. [CrossRef]
59. Yin, J.; Yu, D.; Lin, N.; Wilby, R.L. Evaluating the cascading impacts of sea level rise and coastal flooding on emergency response spatial accessibility in Lower Manhattan, New York City. *J. Hydrol.* **2017**, *555*, 648–658. [CrossRef]
60. Peng, J.; Wei, H.; Wu, W.H.; Liu, Y.X.; Wang, Y. Storm flood disaster risk assessment in urban area based on the simulation of land use scenarios: A case of Maozhou Watershed in Shenzhen City. *Acta Ecol. Sin.* **2018**, *38*, 3741–3755.
61. Hammond, M.J.; Chen, A.S.; Djordjević, S.; Butler, D.; Mark, O. Urban flood impact assessment: A state-of-the-art review. *Urban Water J.* **2015**, *12*, 14–29. [CrossRef]
62. Islam, M.F.; Bhattacharya, B.; Popescu, I. Flood risk assessment due to cyclone-induced dike breaching in coastal areas of Bangladesh. *Nat. Hazards Earth Syst.* **2019**, *19*, 353–368. [CrossRef]
63. Zhang, W.; Villarini, G.; Vecchi, G.A.; Smith, J.A. Urbanization exacerbated the rainfall and flooding caused by hurricane Harvey in Houston. *Nature* **2018**, *563*, 384–388. [CrossRef] [PubMed]
64. Shi, J.; Cui, L.; Ma, Y.; Du, H.; Wen, K. Trends in temperature extremes and their association with circulation patterns in China during 1961–2015. *Atmos. Res.* **2018**, *212*, 259–272. [CrossRef]
65. Jongman, B.; Ward, P.J.; Aerts, J.C. Global exposure to river and coastal flooding: Long term trends and changes. *Glob. Environ. Chang.* **2012**, *22*, 823–835. [CrossRef]
66. Liao, G.; He, P.; Gao, X.; Deng, L.; Zhang, H.; Feng, N.; Zhou, W.; Deng, O. The Production–Living–Ecological Land Classification System and Its Characteristics in the Hilly Area of Sichuan Province, Southwest China Based on Identification of the Main Functions. *Sustainability* **2019**, *11*, 1600. [CrossRef]
67. Ouma, Y.O.; Tateishi, R. Urban flood vulnerability and risk mapping using integrated multi-parametric AHP and GIS: Methodological overview and case study assessment. *Water* **2014**, *6*, 1515–1545. [CrossRef]
68. Wang, X.; Xia, J.; Dong, B.; Zhou, M.; Deng, S. Spatiotemporal distribution of flood disasters in Asia and influencing factors in 1980–2019. *Nat. Hazards* **2021**, *108*, 2721–2738. [CrossRef]
69. Li, C.; Chai, Y.; Yang, L.; Li, H. Spatio-temporal distribution of flood disasters and analysis of influencing factors in Africa. *Nat. Hazards* **2016**, *82*, 721–731. [CrossRef]
70. Ju, H.; Zhang, Z.; Zhao, X.; Wang, X.; Wu, W.; Yi, L.; Wen, Q.; Liu, F.; Xu, J.; Hu, S. The changing patterns of cropland conversion to built-up land in China from 1987 to 2010. *J. Geogr. Sci.* **2018**, *28*, 1595–1610. [CrossRef]
71. Zuo, Y.; Cheng, J.; Fu, M. Analysis of Land Use Change and the Role of Policy Dimensions in Ecologically Complex Areas: A Case Study in Chongqing. *Land* **2022**, *11*, 627. [CrossRef]
72. Szwagrzyk, M.; Kaim, D.; Price, B.; Wypych, A.; Grabska, E.; Kozak, J. Impact of forecasted land use changes on flood risk in the Polish Carpathians. *Nat. Hazards* **2018**, *94*, 227–240. [CrossRef]
73. Aguejdad, R. The Influence of the Calibration Interval on Simulating Non-Stationary Urban Growth Dynamic Using CA-Markov Model. *Remote Sens.* **2021**, *13*, 468. [CrossRef]
74. Cole, S.J.; Moore, R.J. Hydrological modelling using raingauge- and radar-based estimators of areal rainfall. *J. Hydrol.* **2008**, *358*, 159–181. [CrossRef]
75. Adnan, M.S.G.; Abdullah, A.Y.M.; Dewan, A.; Hall, J.W. The effects of changing land use and flood hazard on poverty in coastal Bangladesh. *Land Use Policy* **2020**, *99*, 104868. [CrossRef]

76. Winsemius, H.C.; Jongman, B.; Veldkamp, T.I.; Hallegatte, S.; Bangalore, M.; Ward, P.J. Disaster risk, climate change, and poverty: Assessing the global exposure of poor people to floods and droughts. *Environ. Dev. Econ.* **2018**, *23*, 328–348. [CrossRef]
77. Kawasaki, A.; Kawamura, G.; Zin, W.W. A local level relationship between floods and poverty: A case in Myanmar. *Int. J. Disaster Risk Reduct.* **2020**, *42*, 101348. [CrossRef]